Journal of Solid State Chemistry 181 (2008) 2639–2645

Contents lists available at ScienceDirect

Journal of Solid State Chemistry

journal homepage: www.elsevier.com/locate/jssc

Structural and electronic phase transitions in $Sr_{1-x}Ce_xMnO_3$ perovskites

Brendan J. Kennedy [a,*], Paul J. Saines [a], Qingdi Zhou [a], Zhaoming Zhang [b], Motohide Matsuda [c], Michihiro Miyake [c]

[a] School of Chemistry, The University of Sydney, Sydney, NSW 2006, Australia
[b] Australian Nuclear Science and Technology Organisation, Private Mail Bag 1, Menai, NSW 2234, Australia
[c] Graduate School of Environmental Science, Okayama University, 3-1-1 Tsushima-Naka, Okayama 700-8530, Japan

ARTICLE INFO

Article history:
Received 11 April 2008
Received in revised form
3 June 2008
Accepted 5 June 2008
Available online 14 June 2008

Keywords:
Perovskite
Phase transition
Jahn–Teller effect
Manganese oxide

ABSTRACT

The structures of eight members of the series $Sr_{1-x}Ce_xMnO_3$ with $0.075 \leqslant x \leqslant 0.4$ have been established using synchrotron X-ray powder diffraction. These exhibit the sequence of structures

$$\underset{Pm\bar{3}m}{\text{cubic}} \xrightarrow{x\approx 0.08} \underset{I4/mcm}{\text{tetragonal}} \xrightarrow{x\approx 0.35} \underset{Imma}{\text{orthorhombic}}$$

with increasing Ce content. Unusual peak broadening due to domain wall scattering is observed near the composition-induced first-order cubic–tetragonal transition. The temperature dependence of the structures for three examples $x = 0.1$, 0.2 and 0.35 is described. For the $x = 0.1$ and 0.35 samples evidence for a first-order loss of the orbital ordering associated with a cooperative Jahn–Teller distortion is presented. The onset of the orbitally disordered state is accompanied by a discontinuous reduction in cell volume.

1. Introduction

Understanding the relationships between structure and the magnetic and electronic properties in perovskite manganites remains a significant challenge in condensed matter science, especially when the Jahn–Teller (JT) active Mn(III) d^4 cation is involved. In part this challenge remains because establishing precise and accurate structures of perovskites is often far from trivial [1]. Typically the perovskite manganites do not form diffraction quality single crystals and powder diffraction methods must be utilized. The almost pathological tendency for perovskites to adopt structures with highly pseudo-symmetric cells necessitates the use of very high-resolution diffraction data, as are now available using synchrotron radiation, although such methods are not routinely used. Unfortunately establishing accurate lattice parameters, and even the correct space group, does not always reveal the critical structural distortions that are typically associated with displacement of the oxygen atoms away from high symmetry general positions and structural refinements are required. For such refinements to be successful high-quality diffraction data are essential. A second problem is that most interesting materials are often poised near instability, which may be structural and/or electronic in origin. This is clearly the case for the manganite perovskites. Such instabilities may lead to local strains and/or inhomogeneities that can impact on the diffraction data and preclude precise structural refinements.

The motivation for many of the studies of perovskite manganites with the general formula $A_{1-x}R_xMnO_3$ (A = Ca and Sr; R = lanthanide element) over the past few decades has been to understand the colossal magnetoresistance (CMR), the metal–insulator transition and charge/orbital ordering (CO) found in these oxides [2–5]. It is now widely accepted that these phenomena arise as a consequence of strong correlation between the spin, charge and orbital degrees of freedom in the manganites.

Even the most cursory survey of the vast literature on perovskite manganites reveals numerous anomalies that are worthy of detailed investigations. A case at point is the electron-doped materials based on $Sr_{1-x}Ce_xMnO_3$. The most commonly observed structure for pure $SrMnO_3$ is the four-layer hexagonal perovskite polytype [6–8]. Failure to observe the more typical cubic perovskite can be rationalized by considering that the tolerance factor, t, is too large [9]. One method to decrease t is to reduce some of the Mn(IV) to Mn(III), thereby increasing the average Mn–O bond length. This is often achieved by partially substituting the Sr by a lanthanide [10,11]. Careful control of the synthetic conditions then yields the cubic, rather than hexagonal phase, at low doping levels and this is seen in $Sr_{0.95}Ce_{0.05}MnO_3$ [12]. As the Ce content is increased in $Sr_{1-x}Ce_xMnO_3$ a transition to a tetragonal structure with $c/a \sim 1.018$ is observed [13]. Further doping reduces the magnitude of the tetragonal distortion

* Corresponding author. Fax: +61 2 9351 3329.
E-mail address: B.Kennedy@chem.usyd.edu.au (B.J. Kennedy).

0022-4596/$ - see front matter © 2008 Elsevier Inc. All rights reserved.
doi:10.1016/j.jssc.2008.06.022

(c/a ratio) until near $x\sim0.35$ a transition to an orthorhombic structure occurs [13]. In the simplest case reduction in the tetragonal distortion might presage a transition to cubic, yet in $Sr_{1-x}Ce_xMnO_3$ the transition to cubic occurs close to the composition where the tetragonal lattice distortion is greatest [13]. The cubic to tetragonal structural transition accompanied by the JT transition was also observed in Cr-doped manganites $Sr_{0.95}Ce_{0.05}Mn_{1-y}Cr_yO_3$ ($y = 0$, 0.05 and 0.1), with the transition temperature decreasing with increasing Cr doping [14].

The aim of the present paper is to describe results of a synchrotron X-ray powder diffraction study of the structures and phase transitions in the series $Sr_{1-x}Ce_xMnO_3$ with $0.075 \leqslant x \leqslant 0.4$. We show here that whilst the cell metric approaches higher symmetry with increasing Ce content, the connectivity of the MnO_6 octahedra actually becomes more distorted, ultimately undergoing a first-order tetragonal–orthorhombic transition. The temperature dependence of the structures of three representative examples is also described.

2. Experimental

The $Sr_{1-x}Ce_xMnO_3$ samples (ca. 4 g) were prepared by solid-state reaction. Powders of pre-dried $SrCO_3$ (Kantou kagaku, 99.9%), CeO_2 (Kantou kagaku, 99.99%) and Mn_3O_4 (Koujundo kagaku, 99.9%) were weighed at stoichiometric proportions and mixed for 24 h using a ball mill. The mixture was then heated to 800 °C at 5°/min and next annealed for 10 h in air. The calcined powder was then reground in a ball mill for 24 h, sintered at 1400 °C for 10 h in air and cooled at 5°/min to room temperature. The samples were analysed using a JEOL 6400 scanning electron microscope fitted with a Tracor Northern energy-dispersive spectrometer (EDS) operated at 15 kV. A comprehensive set of standards was used for quantitative work, giving a high degree of accuracy. This verified that the cation ratios were within one ESD of nominal stoichiometry.

Synchrotron X-ray diffraction (XRD) data were collected on the Debye–Scherrer diffractometer at the Australian National Beamline Facility, Beamline 20B at the Photon Factory, Tsukuba, Japan [15]. This diffractometer utilizes a channel-cut Si (111) monochromator that accepts the beam directly from the bending magnet source. The samples were housed in 0.3 mm diameter capillaries that were rotated during the measurements. Data were recorded in the angular range $5 < 2\theta < 85°$, step size 0.01° using two Fuji Bas Image plates. The wavelength of the X-rays was 0.80286 Å, estimated using the NIST Si640c wavelength standard. The diffractometer operates at a vacuum of $\sim10^{-3}$ Torr, this significantly lowering the background from air-scatter, enhancing the ability to detect weak reflections. The accurate measurement of the intensities in these weak reflections is critical for precise structural refinements from the data. Variable temperature data were collected, using a custom-built furnace, at temperatures of up to 800 °C. Refinements of the crystal structures were performed using the program RIETICA [16]. The diffraction peaks were described by a pseudo-Voigt function using a Howard asymmetry correction. The background was estimated from interpolation between up to 40 selected points.

3. Results and discussion

3.1. Room temperature space group and structure

The appropriate space group for the $Sr_{1-x}Ce_xMnO_3$ manganite perovskites was established from consideration of both the observed pattern of splitting of the Bragg reflections from the parent primitive cell and the nature of the superlattice reflections associated with the tilting of the octahedra. The synchrotron diffractometer employed in this study allowed both factors to be well probed. Fig. 1 illustrates portions of the diffraction patterns for the eight $Sr_{1-x}Ce_xMnO_3$ manganite perovskites studied in the present work. In $Sr_{0.925}Ce_{0.075}MnO_3$ ($x = 0.075$) the 211 reflection near $2\theta\sim29.7°$ is a single peak and there is no observed intensity associated with the R-point or M-point modes demonstrating the structure to be cubic. The appropriate space group is $Pm\bar{3}m$. Whilst this choice accounts for all the observed reflections (and does not predict any unobserved reflections), the measured peaks all have a broad and very unusual peak shape. We ascribe this unusual peak shape to the presence of severe strains in the lattice.

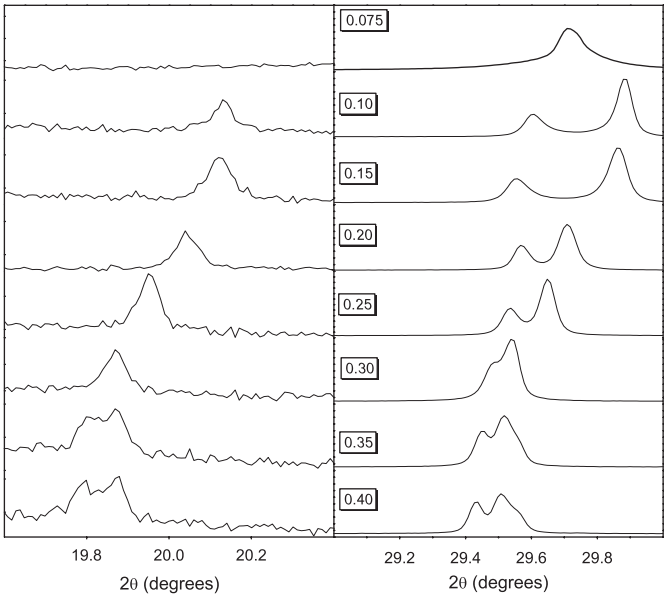

Fig. 1. Portion of the observed synchrotron X-ray powder diffraction patterns for eight members of the series $Sr_{1-x}Ce_xMnO_3$. The R-point reflection near $2\theta\sim20°$ is indicative of out-of-phase tilting of the MnO_6 octahedra and the cubic 211 reflection near $2\theta\sim29.5°$ provides a guide to the cell metric. The intensities of the plots have been scaled to highlight the appropriate features.

At $x = 0.1$, the cubic 211 reflection is split into two well-separated reflections indexed as 204 and 312 for a $\sqrt{2}a_p \times \sqrt{2}a_p \times 2a_p$ superstructure where the subscript p denotes the pseudo-cubic subcell and a number of R-point reflections such as the 121 peak near $2\theta\sim20°$ are clearly evident. Thus, the structure is tetragonal with $c/a > 1$ and has only out-of-phase tilting of the MnO_6 octahedra about the c-axis demonstrating $I4/mcm$ to be the appropriate space group [17]. In Glazer's notation the structure has the $a^0a^0c^-$ tilt system [18]. At $x = 0.35$ the parent 211 reflection is further split as is the R-point reflection near $2\theta\sim20°$, demonstrating that symmetry lower than tetragonal is present. No M-point or X-point reflections are observed in the diffraction pattern and it is deduced that the appropriate space group for this oxide, and for the $x = 0.4$ sample, is $Imma$ [17], with the $a^-b^0a^-$ tilt system. These choices are the same as those made by Sundaresan et al. [13] for $x = 0.1$, 0.2, 0.3 and 0.4 using powder neutron diffraction data. The composition-dependent evolution of the structures in the $Sr_{1-x}Ce_xMnO_3$ series can be summarized as

$$\underset{Pm\bar{3}m}{\text{cubic}} \xrightarrow{x\approx0.08} \underset{I4/mcm}{\text{tetragonal}} \xrightarrow{x\approx0.35} \underset{Imma}{\text{orthorhombic}}$$

This sequence of phases has been observed in a number of perovskite systems including $Sr_{1-x}Ba_xMO_3$ (M = Hf, Zr) [19,20] and in both $SrZrO_3$ [21] and $SrRuO_3$ [22] as a function of temperature. Interestingly the $Imma$ phase is not seen in the

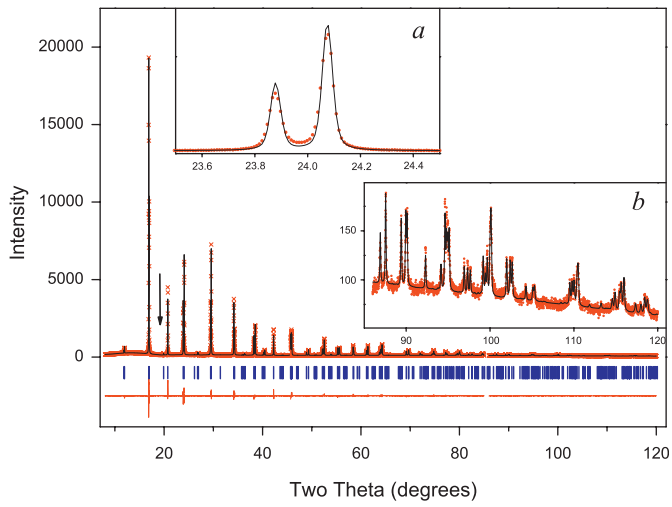

Fig. 2. Observed (crosses), calculated and difference X-ray diffraction profiles for $Sr_{0.8}Ce_{0.2}MnO_3$. The positions of the allowed Bragg reflections are indicated by the short vertical markers. The arrow indicates the position of the 121 *R*-point reflection highlighted in Fig. 1. The insets show (a) the effect of the domain wall broadening on the diffraction pattern, this is mainly responsible for the fluctuations in the difference profile and (b) the quality of the data to high angles.

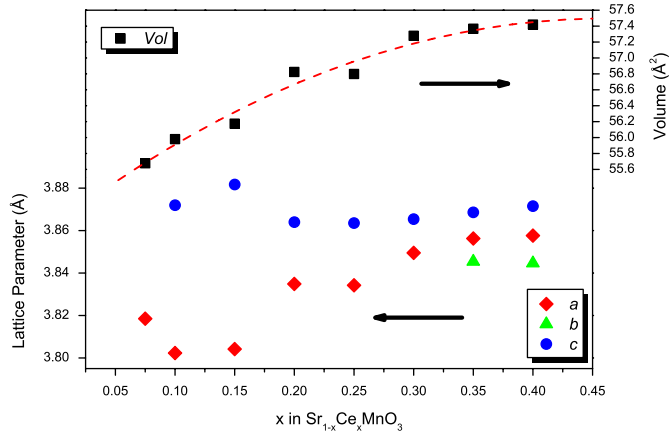

Fig. 3. Composition dependence of the equivalent primitive cell volume and appropriately scaled lattice parameters for $Sr_{1-x}Ce_xMnO_3$ obtained from the Rietveld refinements. The tetragonal I4/*mcm* has a $\sqrt{2}a_p \times \sqrt{2}a_p \times 2a_p$ superstructure and the orthorhombic *Imma* has a $\sqrt{2}a_p \times 2a_p \times \sqrt{2}a_p$ superstructure. The ESDs in the parameters are smaller than the symbols.

pure Mn^{IV} oxides $Sr_{1-x}Ca_xMnO_3$ [23–25] where a first-order *I*4/*mcm*–*Pnma* transition is observed. Indeed although the *Imma* phase features in a number of ABO_3 perovskites containing heavy (second or third row) transition metals and *p*-block (Pb, Sn) metals [26–28], it is only observed for first row TM (Ti and Mn) when an additional, e.g. electronic, effect is present [29–32].

Structures were then refined, in the space groups deduced above, for each of the eight oxides studied, using the Rietveld method. The combination of resolution, signal-to-noise and measured *d*-range of these diffraction measurements typically results in very accurate structural refinements for oxides involving first row TM; see for example our recent studies of $CaMnO_3$ and $Ca_{1-x}Sr_xMnO_3$ [23,24] A representative result from the Rietveld refinements is given in Fig. 2. The evolution of the lattice parameters from these refinements, illustrated in Fig. 3, is similar to, although not identical with, that reported by Sundaresan [13]. We speculate that these minor differences might be a consequence of the different preparative conditions used, noting our samples were annealed at 1400 °C whereas Sundaresan et al. [13] used 1600 °C (the rate of cooling, which was not specified in Ref. [13], might be different as well). Both sets of results demonstrate that as the Ce content (and hence the amount of Mn^{3+} present) increases the volume of the cell shows a systematic increase. This is in accord with the changes in the ionic radii of the species involved {Sr^{2+} 1.44, Ce^{3+} 1.34, Mn^{3+} 0.645 and Mn^{4+} 0.53 Å} [33]. The observed increase in volume indicates that the oxidation state of Ce cannot be all 4+ as proposed in Ref. [34], since the size difference between Sr^{2+} and Ce^{4+} (1.14 Å) is more than twice that of Mn^{3+} and Mn^{4+}, therefore the overall volume would be expected to decrease with increasing Ce^{4+} content. This is consistent with our X-ray photoelectron spectroscopy results (not shown here), which suggest our samples contain predominantly Ce^{3+}. The apparent non-systematic variation in the individual lattice parameters is in marked contrast to the systematic increase in volume. Fig. 3 clearly indicates the *c*/*a* ratio is largest when the tetragonal structure is first observed upon Ce doping, indicative of a first-order $Pm\bar{3}m$–*I*4/*mcm* transition. A second noticeable discontinuity is observed between $x = 0.15$ and 0.2. Finally, there is no obvious discontinuity in the expansion of the cell volume associated with the *I*4/*mcm*–*Imma* transition, similar to that observed in $Ca_{1-x}La_{2x/3}TiO_3$ [35], despite the fact that such a transition must be first order [17].

The observed anomalies in the lattice parameters appear to be associated with a number of features in the shapes of the peaks observed in the diffraction patterns. The experimental set-up typically yields peaks that are predominantly Gaussian in shape and readily modeled using a pseudo-Voigt peak shape [15]. As noted above, and is evident in Fig. 1 the reflections in $Sr_{0.925}Ce_{0.075}MnO_3$ are unusually broad and show a strong Lorentzian character. In general broadening of the peaks in powder diffraction patterns is caused by crystallite size, lattice defects, stress gradients and/or chemical heterogeneities. In the present case we ascribe this broadening to internal strains within the structure brought about by the JT distortion of the Mn^{3+} (d^4) cations. Since the cell metric is cubic there is no obvious easy axis of distortion and whilst it is likely that the MnO_6 octahedra in the cubic structure are distorted on a local scale, there is no long-range ordering of these distortions and this leads to large local stresses resulting in severe peak broadening. A transition to tetragonal allows for long-range ordering of the MnO_6 distortions, significantly reducing the stresses and resulting in more typical peak widths and shapes. Regular packing of elongated octahedra may be favoured in the tetragonal structure and this would be more efficient than random packing as thought to be the case in the cubic structure. This may result in a decrease in volume going from cubic to tetragonal. Recall also that the tolerance factor for the cubic phase of $SrMnO_3$ is unusually high indicating instability.

At $x \sim 0.1$ the JT-induced strain is sufficiently pervasive and long-range ordering of the distortions occur, inducing a transition to tetragonal. That is to say the composition-induced $Pm\bar{3}m$–*I*4/*mcm* transition is driven by the internal strains associated with the JT effect and not the more commonly observed cooperative tilting of the MnO_6 octahedra. Orbital order (JT distortion) and octahedral tilting can co-exist in *I*4/*mcm* and indeed the strength of the *R*-point reflections, shown in Fig. 1, demonstrates that tilting of the MnO_6 octahedra exists at $x = 0.1$ (obviously long-range ordering of the tilts cannot exist in $Pm\bar{3}m$). The tilt angle in the $x = 0.1$ sample is calculated to be 3.9° based on the refined oxygen positional parameters using $\tan\varphi = 4x(O1)-1$. Such tilts alone cannot drive the large tetragonal distortion (Fig. 3). As the Ce, and hence Mn^{3+}, increases, the cell metric distortion decreases but the tilt angle, φ, shows a systematic increase (Fig. 4). Such a disjoint between the crystal structure and internal geometry is quite interesting; the same behaviour is also observed

in a number of other perovskite systems including $Ca_{1-x}La_{2x/3}TiO_3$ [35]. It is worth noting that the progressive increase in the Ce content leads to a larger uncertainty in the refined oxygen positional parameters. The adverse effect of heavy elements on the refinement of structures from XRD is well known (Table 1).

A striking feature of the diffraction pattern of the tetragonal samples with lower Ce contents ($x = 0.1$ and to a less extent 0.15) is the anisotropic peak broadening and large amount of residual intensity between the tetragonal doublets, see Figs. 1 and 2. This is indicative of domain wall effects [36,37]. Near the composition-induced first-order cubic–tetragonal transition, there will be domains of the crystallites having the tetragonal structure, and domains from the cubic phase. On each side of a domain boundary there can either be the cubic phase, or one of six different orientations of the tetragonal phase. The mismatch of the lattices induces large local strains, which will relax to zero at a finite distance away from the domain boundary.

At this stage the precise origin of the discontinuity in the lattice parameters near $x\sim0.2$ is uncertain. Examination of the MnO_6 octahedra shows these to be distorted, with those in $I4/mcm$ showing an elongation of the MnO_6 octahedra. This can be quantified using the relationship $\Delta d = (1/6)\Sigma[(d_n-d)/d]^2$ where d is the mean Mn–O distance and d_n the individual Mn–O distance [38]. This discontinuity in the lattice parameters corresponds to a marked reduction in the distortion of the MnO_6 octahedra (Δd) from $\sim60\times10^{-6}$ for $x\leqslant0.15$ to $\sim2\times10^{-6}$ for $x\geqslant0.2$. This change is comparable with the abrupt decrease of the JT effect observed in other manganites such as $Pr_{0.7}Ca_{0.3}MnO_3$ [39–41]. Further studies

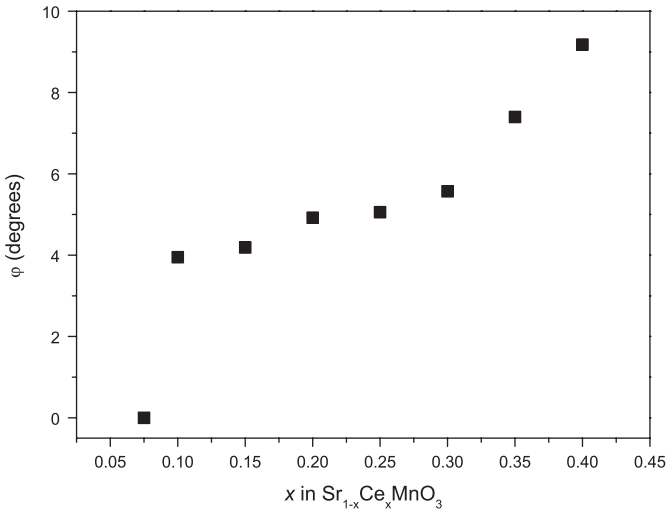

Fig. 4. Composition dependence of the tilt angle φ for the series $Sr_{1-x}Ce_xMnO_3$. In all cases (except cubic) the tilt angle was calculated using the refined atomic coordinates.

are required to establish whether the origin of this anomaly is also due to an anomalous magnetostriction feature.

As the Ce content is increased above 0.3, a first-order transition to the orthorhombic *Imma* phase occurs. Remarkably this transition is not accompanied by a discernable discontinuity on the cell volume but it is accompanied by a discontinuity in the tilt angle (Fig. 4) calculated as $\phi = \frac{1}{2}\{\tan^{-1}[-4\sqrt{2}y(O2)]+\tan^{-1}[2\sqrt{2}z(O1)]\}$ in the *Imma* phase. This contrasts with the behaviour observed in other perovskites that display a first-order phase transition such as $PrAlO_3$ [42] and $Ca_{1-x}La_{2x/3}TiO_3$ [35] where the magnitude of the tilt is essentially identical in both phases, although as occurs here, the tilt axis is different. This suggests that the transition is not solely driven by size effects but rather also has an electronic contribution. The possibility of such a contribution was noted by Sundaresan et al. [13] who, using neutron diffraction, observed a transition from axially elongated to axially compressed octahedra. The current XRD measurements, although giving slightly larger ESDs for the Mn–O bond distances than those reported in this previous work, also show a transition from elongated to compressed octahedra accompanying the tetragonal to orthorhombic transition. Such a reversal in the nature of the octahedral distortion requires a re-distribution of the Mn 3d electrons with the electron switching from the d_z^2 orbital to the $d_x^2-_y^2$-type orbitals.

Clearly the electronic contribution of the JT active Mn^{3+} ions has a significant effect on the details of these phase transitions. As the Ce content increases the amount of the JT active Mn^{3+} ions present increases and one would expect an increase in the tetragonal distortion of the cell. That this is not seen suggests that the increase in the octahedral tilting evident from the structural refinements somehow acts to negate this. This is in contrast to what was observed in rare-earth manganites $RMnO_3$ that octahedral tilting enhanced the magnitude of JT distortion [43].

3.2. Variable temperature studies

The phase transition behaviour of three of the samples, with $x = 0.1$, 0.2 and 0.35, was also investigated using high-temperature XRD. These three compositions provide representative members for the three regions apparent in Fig. 3.

Heating $Sr_{0.8}Ce_{0.2}MnO_3$ to above 400 °C results in a continuous transition from the tetragonal, $I4/mcm$, structure to one in cubic, $Pm\bar{3}m$. This is the same structural sequence found, on heating, in $Sr_{1-x}Pr_xMnO_3$ with $0.075\leqslant x\leqslant0.4$ [10]. As is evident from Fig. 5, increasing temperature results in a progressive loss of the tetragonal splitting in $Sr_{0.8}Ce_{0.2}MnO_3$ with a concurrent decrease in the intensity of the diagnostic *R*-point reflections. It is possible to estimate the transition temperature T_c from either the point in which the *R*-point reflections are no longer observed and/or a loss

Table 1
Selected structural parameters in the series $Sr_{1-x}Ce_xMnO_3$ from refinement of synchrotron X-ray diffraction data

x	Space group	a (Å)	b (Å)	c (Å)	x(O1)[a]	z(O1)	y(O2)	R_p (%)	R_{wp} (%)
0.075	$Pm\bar{3}m$	3.8185(2)			1/2	0		6.12	7.17
0.10	$I4/mcm$	5.3773(1)		7.7440(1)	0.2673(8)			8.86	7.33
0.15	$I4/mcm$	5.3799(1)		7.7634(1)	0.2683(9)			7.45	5.67
0.20	$I4/mcm$	5.4233(1)		7.7279(1)	0.2715(8)			5.04	6.41
0.25	$I4/mcm$	5.4224(1)		7.7271(1)	0.2712(6)			4.39	4.09
0.30	$I4/mcm$	5.4440(1)		7.7307(1)	0.2744(8)			4.04	3.74
0.35	*Imma*	5.4536(1)	7.6908(1)	5.4710(1)		0.0407(14)	−0.0258(7)	3.54	3.25
0.40	*Imma*	5.4555(1)	7.6893(2)	5.4752(1)		0.0576(25)	−0.0283(11)	3.31	3.55

The higher than usual *R* parameters in the cubic and tetragonal phases reflect the impact of domain wall broadening.
[a] In $I4/mcm$ the O1 atom is at $xx+\frac{1}{2}0$ and O2 is at $00\frac{1}{4}$ and in *Imma* O1 is at $0\frac{1}{4}z$ and O2 is at $\frac{1}{4}y\frac{1}{4}$. In both space groups the Mn is at 000.

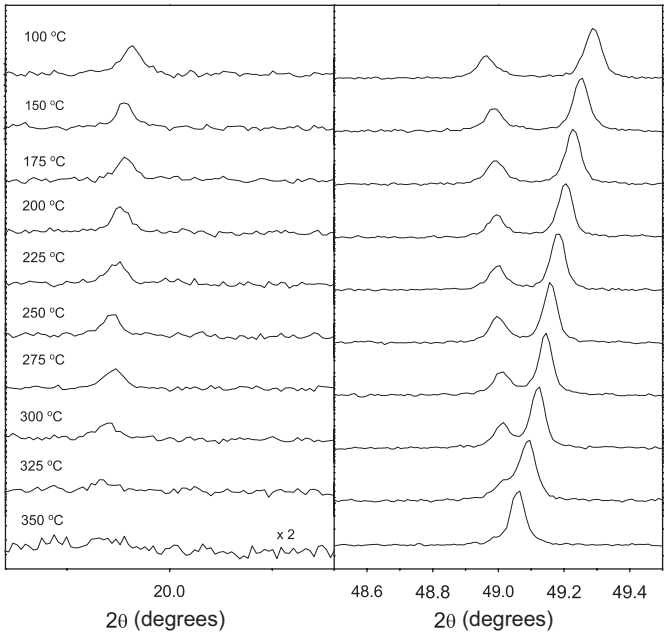

Fig. 5. Portion of the observed synchrotron X-ray powder diffraction patterns for $Sr_{0.8}Ce_{0.2}MnO_3$ as a function of temperature. The *R*-point reflection near $2\theta \sim 20^\circ$ is indicative of out-of-phase tilting of the MnO_6 octahedra and the cubic 4 0 0 reflection near $2\theta \sim 49^\circ$ provides a guide to the cell metric. The *R*-point reflection is lost at about the same temperature as the splitting of the 4 0 0 reflection is lost.

of resolved tetragonal splitting. Both these measures suggest the transition to cubic occurs near 385 °C.

Further insight into the phase transition can be obtained through analysis of the spontaneous strains. The thermally induced ferroelastic $Pm\bar{3}m$–$I4/mcm$ transition has been observed in numerous perovskites [1], the most comprehensively studied example of which is $SrTiO_3$ [44]. A key feature of this type of transition is that the volume does not change through the structural phase transition. The transition to the tetragonal structure in $Sr_{0.8}Ce_{0.2}MnO_3$ is characterized by tilting of the MnO_6 octahedra around $[001]_p$, that introduces spontaneous strains. The spontaneous strains are quantified by the expression $\varepsilon_t = (c_p - a_p)/a_0$ where a_p and c_p are the pseudo-cubic subcell lengths and a_0 is the reference parameter for the cubic structure, or if a_0 cannot be accurately estimated, the strain can be approximated by $\varepsilon_t = (c_p - a_p)/((1/2)/(a_p + c_p))$ [45]. The temperature dependence of the lattice parameters (Fig. 6) for $Sr_{0.8}Ce_{0.2}MnO_3$ is that expected for a continuous phase transition. The plot of the tetragonal strain, ε_t, vs T is linear, Fig. 7, and suggests a transition temperature of 388 °C.

The temperature dependence of the lattice parameters for the $x = 0.1$ sample $Sr_{0.9}Ce_{0.1}MnO_3$ (Fig. 8) appears, at first, to be very similar to that seen for the $x = 0.2$ sample described in detail above. That is there is a systematic decrease in c_p and increase in a_p approaching the $I4/mcm$ to $Pm\bar{3}m$ transition resulting in a linear dependence of the strain on temperature (Fig. 9). The transition temperature estimated from the strain is 214 °C. The pattern recorded at 215 °C shows no evidence for any peak broadening or asymmetry, or for intensity at the *R*-point superlattice reflections, consistent with this. This behaviour is very different to the results reported by Hashimoto and Iwahara [46] who found that $Sr_{0.9}Ce_{0.1}MnO_{3-\alpha}$ undergoes a first-order $I4/mcm$ to $Pm\bar{3}m$ transition near 50 °C. The description of the electron diffraction patterns for $Sr_{0.9}Ce_{0.1}MnO_3$ by Sundaresan et al. [13] are consistent with a continuous transition near 70 °C. This variation in both the nature and temperature of the transition to the cubic structure suggests that it is very sensitive to the precise

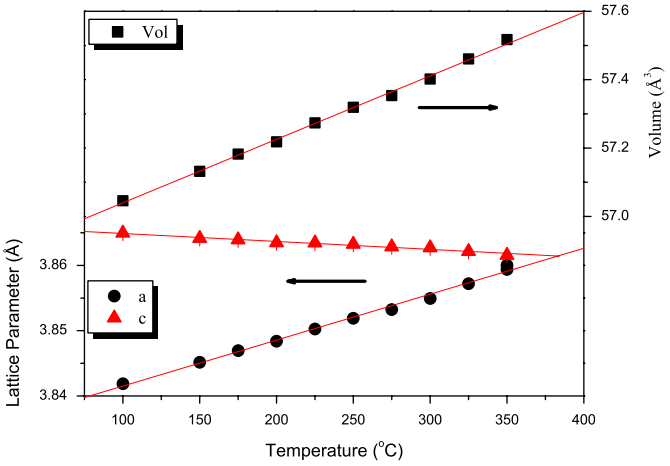

Fig. 6. Temperature dependence of the equivalent primitive cell volume and appropriately scaled lattice parameters for $Sr_{0.8}Ce_{0.2}MnO_3$ obtained from the Rietveld refinements. The ESDs in the parameters are smaller than the symbols.

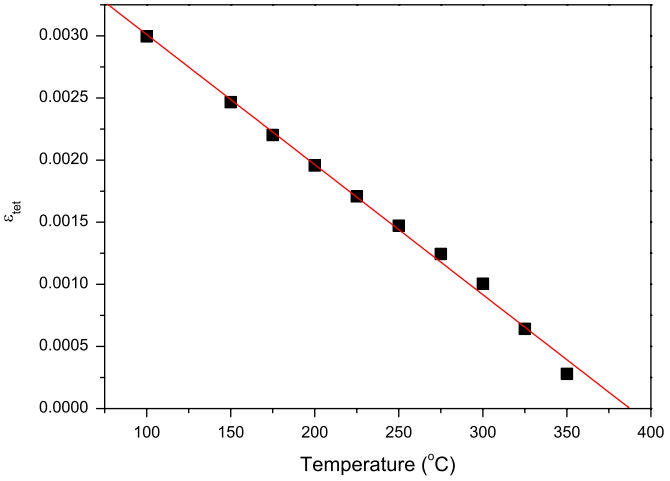

Fig. 7. Plot of temperature dependence of the tetragonal strain for $Sr_{0.8}Ce_{0.2}MnO_3$. The linear dependence shows the transition to be continuous with a transition temperature of 388 °C.

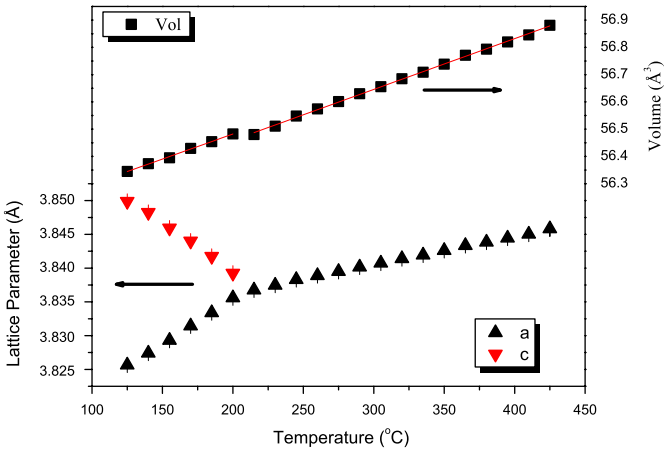

Fig. 8. Temperature dependence of the equivalent primitive cell volume and appropriately scaled lattice parameters for $Sr_{0.9}Ce_{0.1}MnO_3$ obtained from the Rietveld refinements. Note the small discontinuity in the volume near 210 °C. The ESDs in the parameters are smaller than the symbols.

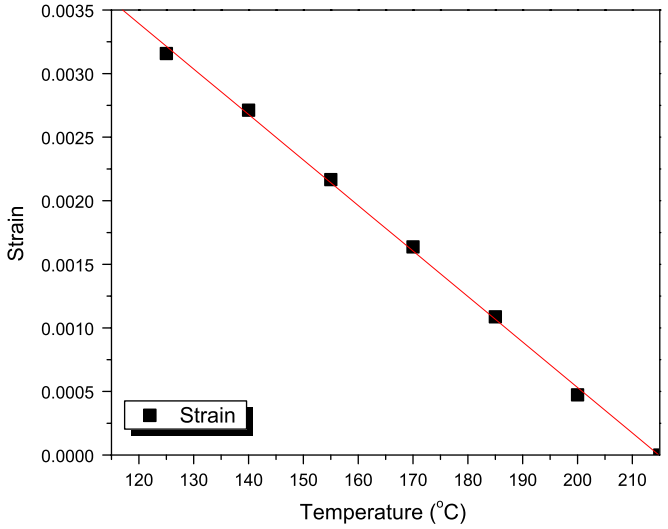

Fig. 9. Temperature dependence of the tetragonal strain in $Sr_{0.9}Ce_{0.1}MnO_3$. The solid line is a linear fit to the observed strain, with $T_c = 214$ °C.

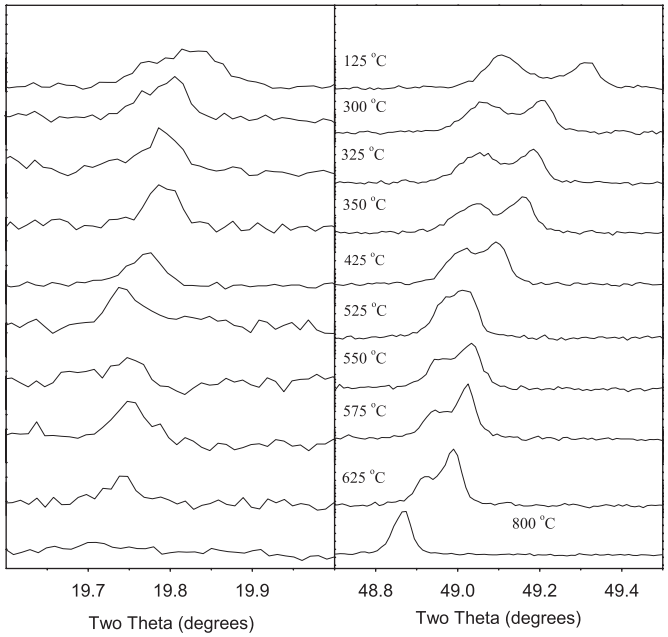

Fig. 10. Portion of the observed synchrotron X-ray powder diffraction patterns for $Sr_{0.65}Ce_{0.35}MnO_3$ as a function of temperature from 125 to 800 °C.

stoichiometry of the material. The intensities of the *R*-point reflections in the tetragonal structure showed a systematic decrease with increasing temperature indicating a reduction in the magnitude of the MnO_6 tilting, however, the ESDs associated with the refined oxygen positional parameters were sufficiently large to preclude a meaningful analysis of the temperature dependence of the tilts. For example at 155 °C, $x(O1) = 0.2626(20)$.

Both above and below the transition temperature the volume shows a linear dependence on temperature for the $x = 0.1$ sample, however there is a small, but noticeable discontinuity in volume at the transition point. It is possible that this volume drop is associated with the suppression of the cooperative JT distortion (CJTD) as has been seen in $LaMnO_3$ [47] and $KCrF_3$ [48], which was attributed to the more efficient packing of the MnO_6 [47] or CrF_6 [48] octahedra in the orbitally disordered state.

The room temperature structure of the $x = 0.35$ sample $Sr_{0.65}Ce_{0.35}MnO_3$ was fitted in the orthorhombic space group *Imma* in response to the observed splitting of both the 2 1 1 reflection near $2\theta \sim 29.5^\circ$ and the *R*-point reflection near $2\theta \sim 19.8^\circ$ (Fig. 1). In *Imma* this *R*-point superlattice reflection appears as a triplet (112/221/031) whereas in *I*4/*mcm* it is a singlet (121). The cubic 4 0 0 reflection at $2\theta \sim 49^\circ$ appears as a doublet in both *Imma* and *I*4/*mcm*, but in *Imma* the lower angle 4 0 4 reflection is stronger than the 0 8 0 reflection, whereas in *I*4/*mcm* the higher angle 4 4 0 reflection is stronger than the 0 0 8 reflection. This reversal of the relative intensities occurs near 325 °C, the same temperature where the *R*-point reflection sharpens (Fig. 10). The pattern at 325 °C was, in fact, best fitted using a two-phase mixture of *I*4/*mcm* and *Imma*. The co-existence of these two phases shows the transition between them to be first order, and this is clearly evident in Fig. 11. This transition is accompanied by a large axial distortion of the MnO_6, suggesting that the tilting about the $[001]_p$ direction in *I*4/*mcm* enhances the magnitude of the JT distortion. In *Imma* the tilting is about $[101]_p$ and this does not give the same synergy to the JT distortion. The distortion Δd, defined as before, increases from 0.8×10^{-6} at 300 °C to 288.6×10^{-6} at 350 °C.

As the temperature is increased above 350 °C there is an obvious reduction in the magnitude of the tetragonal splitting, although the pattern recorded at 800 °C is still indicative of a tetragonal structure. A second striking feature in Fig. 11 is the anomaly in the thermal expansion of a_p in the tetragonal phase

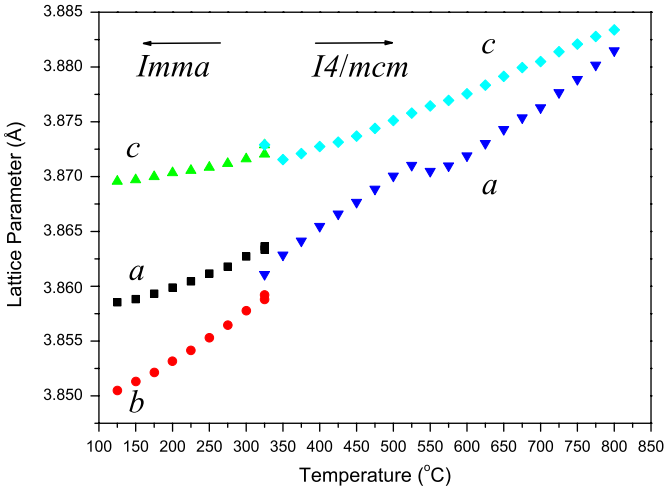

Fig. 11. Temperature dependence of the lattice parameters in $Sr_{0.65}Ce_{0.35}MnO_3$. The *Imma* and *I*4/*mcm* phases co-exist at 325 °C. The ESDs in the parameters are smaller than the symbols.

near 525 °C. This is reflected in the increased splitting of the 4 4 0 and 0 0 8 reflections between 525 and 550 °C in Fig. 10. The thermal expansion of the cell shows the similar anomaly, with the volume of the cell showing a noticeable reduction between 525 and 550 °C. There is no such anomaly or discontinuity in the thermal expansion at the *Imma*–*I*4/*mcm* transition, indeed the volume in the range 125–525 °C is well fitted by a simple quadratic of the form $Vol = 54.38 + 6.630 \times 10^{-4}T + 1.314 \times 10^{-6}T^2$. The abrupt reduction in volume in this sample is reminiscent of that seen in $Sr_{0.9}Ce_{0.1}MnO_3$ near 210 °C and it is ascribed to a similar feature, that is, a first-order quenching of the CJTD. Surprisingly this is not evident in the anisotropy of the bond distances, however, it should be recalled that the octahedral tilting induces a distortion of the octahedra even in the absence of electronic effects.

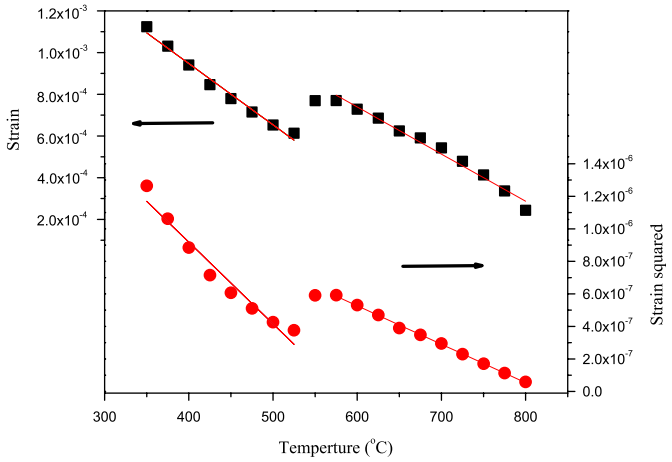

Fig. 12. Temperature dependence of the tetragonal strain and square of the tetragonal strain in the *I*4/*mcm* and *Imma* phases of $Sr_{0.65}Ce_{0.35}MnO_3$.

Additional information on this 525 °C anomaly comes from examination of the tetragonal strain. As is evident from Fig. 12 there is a clear discontinuity in the strain near 525 °C. Below this the strain varies linearly with temperature whereas above 525 °C the square of the strain is linearly dependent on temperature.

4. Conclusion

Doping the cubic polytype of $SrMnO_3$ with Ce to form $Sr_{1-x}Ce_xMnO_3$ induces two first-order phase transitions, initially to *I*4/*mcm* and then to *Imma*. The first of these just below $x = 0.1$ appears to involve both long-range ordering of the JT elongated octahedra and cooperative tilting of the octahedra. The second transition near $x = 0.35$ involves a re-orientation of the MnO_6 tilts from about $[001]_p$ to $[101]_p$. Both structures allow tilting of the MnO_6 octahedra. Although the cell metric apparently approaches higher symmetry with increasing Ce doping, the refined structures show an increase in the magnitude of the tilts.

Heating the samples with $x = 0.1$ and 0.2 results in transition to the cubic $Pm\bar{3}m$ structure at 210 and 385 °C, respectively. Both transitions are continuous with the tetragonal strain showing a linear dependence on temperature. For the $x = 0.1$ sample a discontinuity in volume at the transition to cubic is observed that is due to a first-order quenching of the JT distortion. A first order *Imma*–*I*4/*mcm* transition is observed near $T = 325$ °C in the $x = 0.35$ sample. An anomaly in the thermal expansion of the high temperature tetragonal phase is observed near 525 °C. This anomaly involves an abrupt reduction in cell volume. The nature of the tetragonal strain alters at this point; ε_t vs T is linear below 325 °C but ε_t^2 vs T is linear above this.

Acknowledgments

This work was supported by a grant from the Australian Research Council. Synchrotron diffraction measurements were performed at the Australian National Beamline Facility (ANBF) with support from the Australian Synchrotron Research Program, which is funded by the Commonwealth of Australia under the Major National Research Facilities Program. We thank Dr. Chris Howard for alerting us to this system and for careful reading of the manuscript. The authors gratefully acknowledge the assistance of Dr. James Hester at the ANBF.

References

[1] R.H. Mitchell, Perovskites Modern and Ancient, Almaz Press Inc., Ontario, 2002.
[2] See for reviews in: C.N.R. Rao, B. Raveau (Eds.), Colossal Magnetoresistance, Charge Ordering and Related Properties of Manganese Oxides, World Scientific, Singapore, 1998.
[3] J.B. Goodenough, Phys. Rev. 164 (1967) 785.
[4] A.P. Ramirez, J. Phys.: Condens. Matter 9 (1997) 8171.
[5] T. Wu, S.B. Ogale, J.E. Garrison, B. Nagaraj, Amlan Biswas, Z. Chen, R.L. Greene, R. Ramesh, T. Venkatesan, A.J. Millis, Phys. Rev. Lett. 86 (2001) 5998.
[6] P.D. Battle, T.C. Gibb, C.W. Jones, J. Solid State Chem. 74 (1988) 60.
[7] T. Negas, R.S. Roth, J. Solid State Chem. 1 (1970) 409.
[8] K. Kuroda, N. Ishizawa, N. Mizutani, M. Kato, J. Solid State Chem. 38 (1981) 297.
[9] R.S. Tichy, J.B. Goodenough, Solid State Sci. 4 (2002) 661.
[10] K. Knizek, J. Hejtmanek, Z. Jirak, C. Martin, M. Hervieu, B. Raveau, G. Andre, F. Bouree, Chem. Mater. 16 (2004) 1104.
[11] K. Kikuchi, H. Chiba, M. Kikuchi, Y. Syono, J. Solid State Chem. 146 (1999) 1.
[12] H.Y. Wu, K.Q. Ruan, S.L. Huang, Z.M. Lv, L.Z. Cao, Solid State Commun. 141 (2007) 198.
[13] A. Sundaresan, J.L. Tholence, A. Maignan, C. Martin, M. Hervieu, B. Raveau, E. Suard, Eur. Phys. J. B 14 (2000) 431.
[14] W.J. Lu, Y.P. Sun, X.B. Zhu, W.H. Song, J.J. Du, Phys. Lett. A 349 (2006) 388.
[15] T.M. Sabine, B.J. Kennedy, R.F. Garrett, G.J. Foran, D.J. Cookson, J. Appl. Crystallogr. 28 (1995) 513.
[16] B.A. Hunter, C.J. Howard, A Computer Program for Rietveld Analysis of X-ray and Neutron Powder Diffraction Patterns, Lucas Heights Laboratories, 1998.
[17] C.J. Howard, H.T. Stokes, Acta Crystallogr. B 54 (1998) 782.
[18] A.M. Glazer, Acta Crystallogr. B 28 (1972) 3384;
A.M. Glazer, Acta Crystallogr. A 31 (1975) 756.
[19] L. Li, B.J. Kennedy, Y. Kubota, K. Kato, R.F. Garrett, J. Mater. Chem. 14 (2004) 263.
[20] B.J. Kennedy, C.J. Howard, G.J. Thorogood, J.R. Hester, J. Solid State Chem. 161 (2001) 106.
[21] C.J. Howard, K.S. Knight, B.J. Kennedy, E.H. Kisi, J. Phys.: Condens. Matter 12 (2000) L677.
[22] B.J. Kennedy, B.A. Hunter, J.R. Hester, Phys. Rev. B 65 (2002) 224103.
[23] Q. Zhou, B.J. Kennedy, J. Phys. Chem. Solids 67 (2006) 1595.
[24] Q. Zhou, B.J. Kennedy, J. Solid State Chem. 179 (2006) 3568.
[25] O. Chmaissem, B. Dabrowski, S. Kolesnik, J. Mais, D.E. Brown, R. Kruk, P. Prior, B. Pyles, J.D. Jorgensen, Phys. Rev. B 64 (2001) 134412.
[26] J.R. Hester, C.J. Howard, B.J. Kennedy, R. Macquart, Aust. J. Chem. 55 (2002) 543.
[27] W.T. Fu, D. Visser, D.J.W. IJdo, Solid State Commun. 134 (2005) 647.
[28] E.H. Mountstevens, J.P. Attfield, S.A.T. Redfern, J. Phys.: Condens. Matter 15 (2003) 8315.
[29] M.A. Carpenter, C.J. Howard, K.S. Knight, Z. Zhang, J. Phys.: Condens. Matter 18 (2006) 10725.
[30] P. Ranson, R. Ouillon, J.P. Pinan-Lucarre, P. Pruzan, S.K. Mishra, R. Ranjan, D. Pandey, J. Raman Spectrosc. 36 (2005) 898.
[31] P.M. Woodward, T. Vogt, D.E. Cox, A. Arulraj, C.N.R. Rao, P. Karen, A.K. Cheetham, Chem. Mater. 10 (1998) 3652.
[32] V. Caignaert, F. Millange, M. Hervieu, E. Suard, B. Raveau, Solid State Commun. 99 (1996) 173.
[33] R.D. Shannon, Acta Crystallogr. A 32 (1976) 751.
[34] P. Mandal, A. Hassen, A. Loidl, Phys. Rev. B 69 (2004) 224418.
[35] Z. Zhang, G.R. Lumpkin, C.J. Howard, K.S. Knight, K.R. Whittle, K. Osaka, J. Solid State Chem. 180 (2007) 1083.
[36] H. Boysen, Z. Kristallogr. 220 (2005) 726.
[37] S.R. Andrews, R.A. Cowley, J. Phys. C 19 (1986) 615.
[38] J.A. Alonso, M.J. Martinez-Lope, M.T. Casais, M.T. Fernandez-Diaz, Inorg. Chem. 39 (2000) 917.
[39] D.E. Cox, T. Iglesias, E. Moshopoulou, K. Hirota, K. Takahashi, Y. Endoh, Phys. Rev. B 64 (2001) 024431.
[40] B.A. Hunter, B.J. Kennedy, T. Vogt, Phys. Rev. B 69 (2004) 020410.
[41] V. Caignaert, E. Suard, A. Maignan, Ch. Simon, B. Raveau, C. R. Acad. Sci. Paris 321 (1995) 515.
[42] M.A. Carpenter, C.J. Howard, B.J. Kennedy, K.S. Knight, Phys. Rev. B 72 (2005) 024118.
[43] M.W. Lufaso, P.M. Woodward, Acta Crystallogr. B 60 (2004) 10.
[44] M.A. Geday, A.M. Glazer, J. Phys.: Condens. Matter 16 (2004) 3303.
[45] M.A. Carpenter, in: S.A.T. Redfern, M.A. Carpenter (Eds.), Transformation Processes in Minerals, The Mineralogical Society of America, Washington, DC, 2000, p. 35.
[46] S. Hashimoto, H. Iwahara, Mater. Res. Bull. 35 (2000) 2253.
[47] T. Chatterji, F. Fauth, B. Ouladdiaf, P. Mandal, B. Ghosh, Phys. Rev. B 68 (2003) 052406.
[48] S. Margadonna, G. Karotsis, J. Mater. Chem. 17 (2007) 2013.